Turbulence, Heat and Mass Transfer 7

On the transient modelling of impinging jets heat transfer. A practical approach

M. Bovo[1,2] and L. Davidson[1]
[1]*Dept. of Applied Mechanics, Chalmers University of Technology, Gothenburg, Sweden,* bovo@chalmers.se
[2]*Powertrain Analysis, Volvo Car Corporation, Gothenburg, Sweden*

Abstract – This work compares a number of CFD transient models of an impinging jet with both LES and URANS models. The specific case considered is that of an impinging jet with H/D = 6 and Re 23000. The study spans over a wide number of variables for the purpose to access and directly compare different approaches. The variables tested are: turbulence model (LES Smagorinsky, standard low Reynolds k-ε and V2F), numerical discretization schemes, mesh density (total cell number and local cell distribution), synthetic turbulence inlet fluctuations. The model assessment is based on the comparison with available experiments for wall heat transfer and flow turbulent quantities. The computational cost is also considered for completeness.

1 Introduction

Impinging jet flow has remarkable effects on convective heat transfer. Indeed, this kind of flow has the highest known levels of Nusselt number (Nu) for single phase flows. Figure 1 collects an overview of the flow structures characterizing impinging jets.

Impinging jets have been historically studied analytically and experimentally. Later, also numerical simulations have been deployed in this field with varying degrees of success e.g. [5, 6, 8, 10].

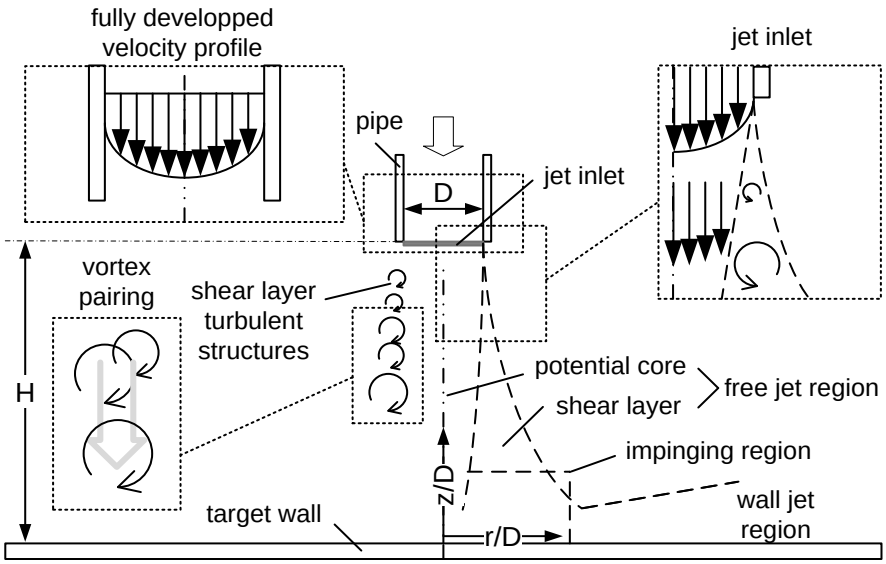

Figure 1: Physics of impinging jets.

This work compares a number of CFD (Computational Fluid Dynamics) transient models of an impinging jet with both LES (Large Eddy Simulation) and URANS (Unsteady RANS) models. The specific case considered is that of an impinging jet with H/D = 6 and Re 23000.

The study spans over a number of variables with the purpose to access and directly compare different approaches. The variables tested are: turbulence model (LES Smagorinsky, standard low Reynolds k-ε and V2F), numerical discretization schemes, mesh (both global and local cell density distribution) and synthetic turbulence inlet fluctuations.

2 Modeling methodology

2.1 Mesh

The mesh size distribution in the wall normal direction has a strong effect on the results. Three meshes are generated by extrusion of parallel layers, the first cell layer is thin enough to guarantee a $z^+<1$ at all-time and every location (see Figure 2, note the z^+ lines). The mesh size in radial and azimuthal direction (stream-wise and span-wise direction) is respectively ~100 and ~30 viscous units in the investigated region.

Figure 2 compares details about the different meshes used. Mesh 1 has a sharp increase in grid spacing in the wall normal direction around z/D=0.5. Mesh 2 has a constant growth with ratio 1.06. These two meshes have ~2e6 cells. Mesh 3 grows as mesh 2 but keeps constant size from about z/D=1.7 upwards resulting in ~2.5e6 cells. The three meshes have the same mesh distribution for z/D<0,5. Mesh 1 is used unless otherwise stated.

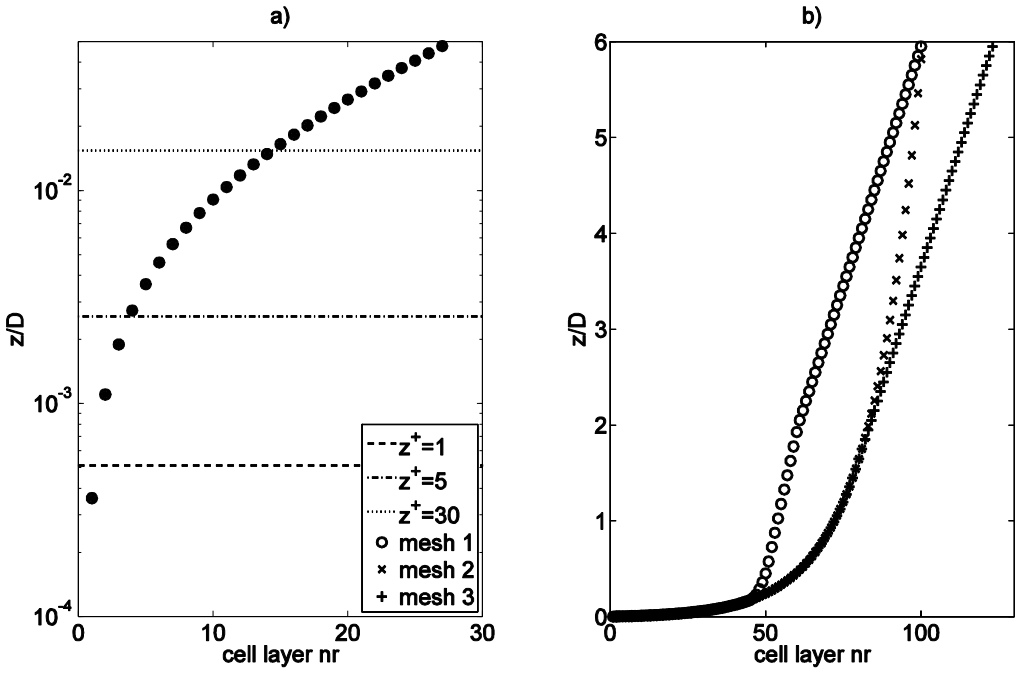

Figure 2: Mesh distribution in wall normal direction. Note: z^+ values are reported.

2.2 Boundary conditions

The outlet boundary condition is *constant pressure.* The impingement wall boundary condition is constant heat flux. The inlet boundary condition is based on a pipe fully developed velocity profile upon which synthetic turbulent velocity fluctuations are superimposed using the method reported in [9] and further discussed in the results section.

2.3 Turbulence models

2.3.1 k-ε

The k-ε belongs to the two-equations model family. A basic assumption for these models is that the effect of turbulence is accounted for with a scalar isotropic property called turbulent viscosity μ_t (i.e. Bousinnesq approximation). Turbulent viscosity is calculated locally in the computational domain and is related to the local turbulent length and velocity scales. The production terms in the transport equation of turbulent quantities are related to the local gradients of the mean flow. The turbulent viscosity μ_t, is derived from the turbulent kinetic energy k and the turbulent dissipation rate ε. Transport equations for these two quantities (k and ε) are resolved along with the momentum and energy equations.

A rather extensive study of two-equations models applied to impinging jets is presented in [10]. The general conclusion of the study is that this type of models is not particularly suitable to solve impinging jet flows. In the same work, the specific results for impinging jets with characteristics similar to the present study indicates that the standard k-ε model performs best, giving the heat transfer prediction closest to the experimental data. Besides, the k-ε model is the most popular of the turbulence models used in industry. For these reasons this model is considered in this investigation.

2.3.2 V2F

The pressure strain affects the turbulent structures in the impinging and wall jet regions of an impinging jet. The V2F model differs from the k-ε model in that it solves for two extra quantities, the wall-normal Reynolds stress v^2, and f_{22}, which is an equation related to the pressure-strain term in the v^2 equation. The V2F model detects the presence of a wall through the f_{22} equation and accounts for its effect on the turbulence.

2.3.3 LES

In a turbulent flow it is possible to distinguish the turbulent structures (eddies) based on their size. The largest eddies are often well recognizable structures in the mean flow; these structures extract kinetic energy from the mean flow field gradient. The largest eddies size is in the order of the geometry and their time scale in the order of the mean flow. The energy collected in the large eddies is passed down to smaller and smaller eddies. In this cascade it becomes more and more difficult to distinguish the turbulent structures and the isotropic assumption becomes more representative. In the smallest eddies the energy is dissipated by viscous effects and goes to increment the flow internal energy (heat).

The basic idea behind LES models is to resolve the large turbulent scales. Consequently, it is necessary to run a three-dimensional, time-dependent computation with a mesh fine enough to capture the large eddies. The effects of eddies with smaller length scales are accounted for with a sub-grid model. LES models differ in how the small eddies are modeled. In this work we use the Smagorinsky sub-grid model because it is the simplest and most commonly used.

3 Results

All results are presented as a statistical relevant average. The quantities describing the turbulence in the jet flow are normalized with the jet bulk velocity at the nozzle outlet W_b. The simulation time step is chosen so that the CFL number is around one for most of the domain, allowing temporary local maxima of ~10.

3.1.1 Effects of numerical discretization

The simulations are carried out using the commercial code Star-CD version 4.12. This commercial code can be run with its own patented second order discretization scheme called MARS (Monotone Advection and Reconstruction Scheme). Three cases are run using LES with values for the MARS parameter of 0, 0,25 and 0,5. A low value for the MARS parameter dampens the resolved turbulence fluctuations with a clear trend particularly for the wall normal velocity fluctuation w'w' at r/D=0 (see Figure 3). On the other hand, no sensible difference or trend is appreciated on the average Nu (Figure 4).

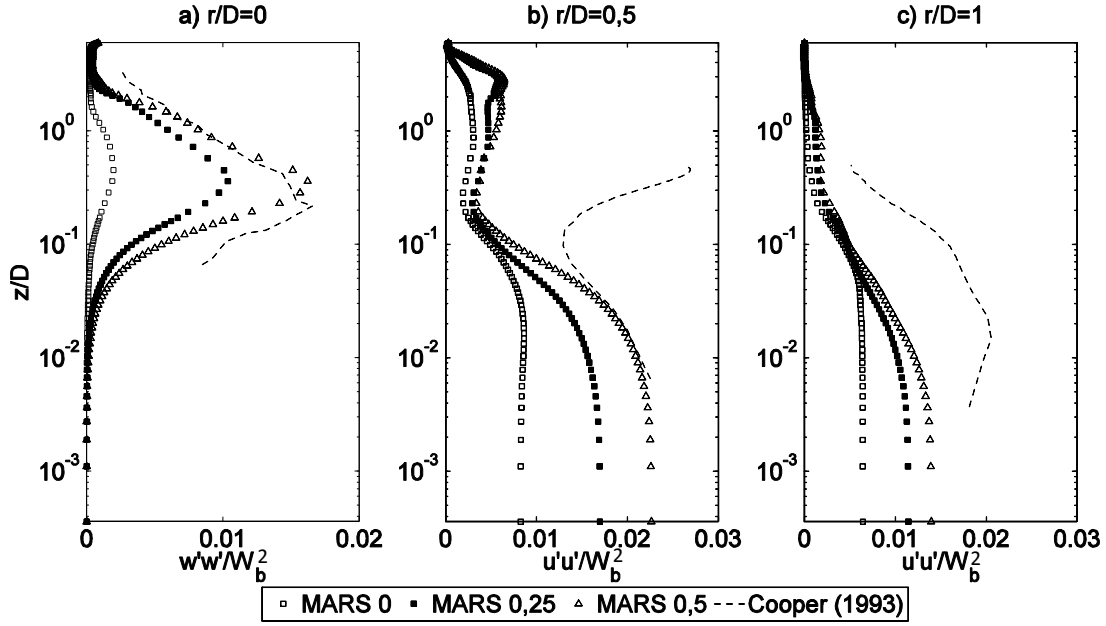

Figure 3: Effects of discretization scheme on velocity fluctuations. w' (wall normal) and u' (radial) velocity fluctuation.

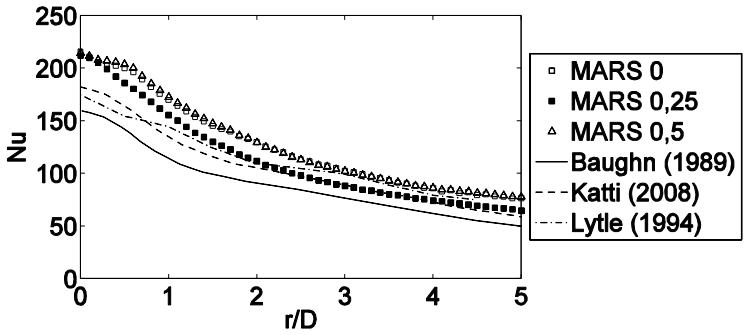

Figure 4: Effect of discretization scheme on Nu.

In the literature, use of the central difference scheme is recommended for LES simulations at least for the momentum equations. A few attempts to apply this scheme gave no good results generating unphysical values for the Nu. In the simulation below, MARS 0,25 is used as default value to enhance the likelihood to achieve convergence.

3.1.2 Effect of inlet turbulence

The inlet turbulent fluctuations are calculated using the method presented in [9]. The method is specifically design to generate inlet boundary conditions to LES. The turbulent integral

length scale and time scale are derived from the inlet size and wall shear stress. A number of independent velocity fluctuation fields are produced based on the turbulent integral length scale. The fields are independent in the sense that their time correlation is zero. These are interpolated using a so called "asymmetric time filter" (a weighted interpolation of the velocity fluctuations based upon the turbulent integral time scale and the simulation time step). The interpolated turbulent velocity fluctuations are then superimposed to the averaged fully developed velocity profile at the inlet.

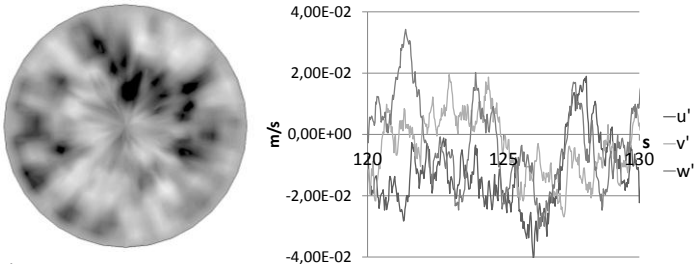

Figure 5: Example of synthetic fluctuations to be superimposed at the inlet. (left) instantaneous inlet u' field and (right) time resolved fluctuations at one inlet boundary cell.

To study the effect of inlet turbulence, cases are run respectively with 25% and 400% of the nominal value for k at the inlet. A rapid decrease in resolved k is observed close to the inlet for r/D=0 (Figure 6). For r/D=0,5 (i.e. nozzle edge) the turbulent fluctuations grow very rapidly with the resolved turbulence growing up to one order of magnitude compared to the levels at the inlet. This effect largely overcomes the inlet turbulence at r/D=0 when the shear layer reaches the jet centrum at about z/D=3. A similar effect can be noticed at r/D=1 where the resolved turbulence is almost zero until the shear layer effects are felt at about z/D=2,5. Consequently the inlet turbulence level has little effects on the average Nu being dominated by the shear layer turbulence. Only close to the impinging zone (r/D<0,5) it is possible to find a correlation growing Nu and inlet turbulence (Figure 7). Farther away from the impingement point the simulations result closely follow the experimental data.

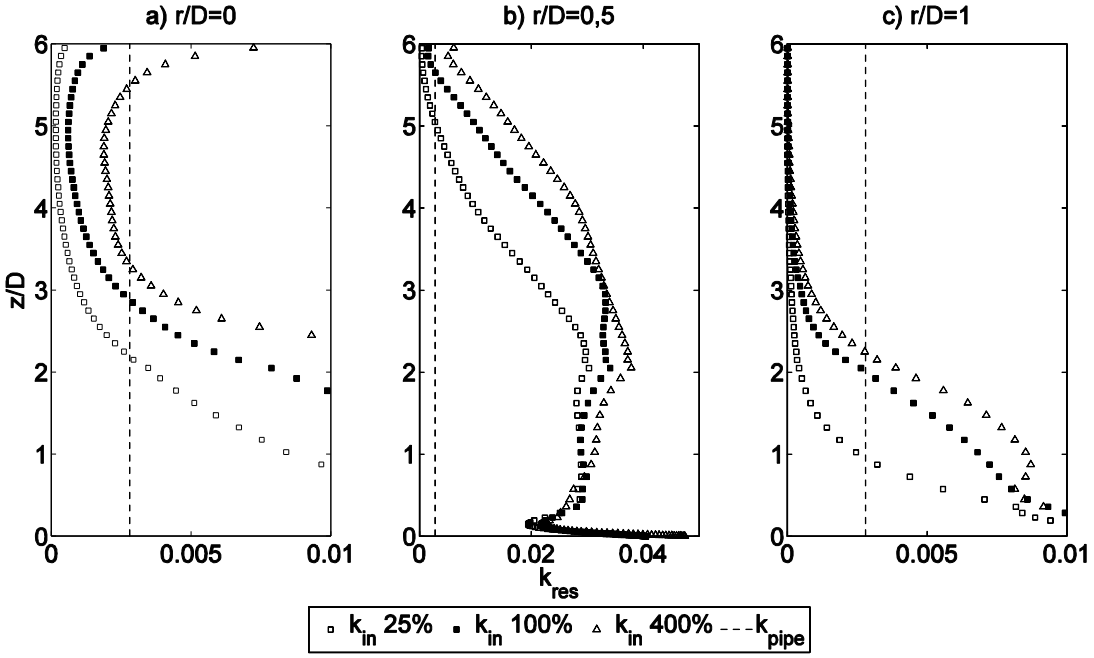

Figure 6: Effects of inlet turbulence on resolved k (k_{res}). Fully developed pipe flow "k_{pipe}".

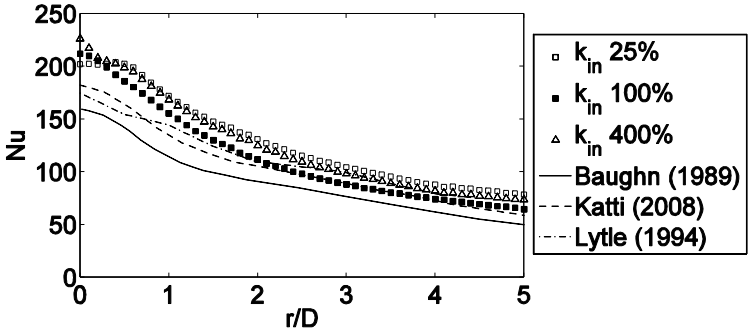

Figure 7: Effect of inlet turbulence on Nu.

The behavior described above is confirmed by the plots of specific velocity fluctuations (Figure 8). The inlet synthetic fluctuations have appreciable effects only in the potential core r/D=0 where the case with nominal values of turbulence (k_{in} 100%) matches best the experimental results in both magnitude and shape.

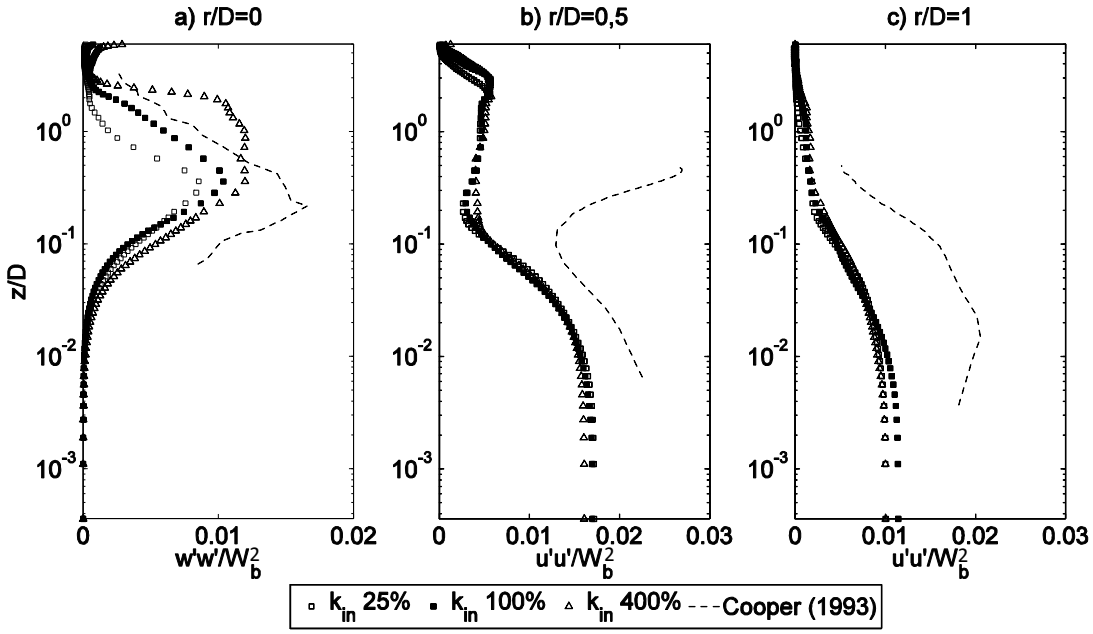

Figure 8: Effects of inlet turbulence on resolved velocity fluctuations. w' (wall normal) and u' (radial) velocity fluctuation.

3.2 Mesh size effects

3.2.1 Effects of mesh global and local density.

Three meshes are tested using the LES model with similar number of cells but different distribution in wall-normal direction (mesh 1, mesh 2 and mesh 3). See Figure 2 for details on the mesh distribution.

Figure 9 shows the effect of cell size on the turbulent fluctuations near the inlet. Mesh 2 has bigger, more elongated, cells close to the inlet and results in an evident dampening effect on the turbulent fluctuations. For all meshes there is a rapid decrease in velocity fluctuations along the flow direction for r/D=0. With mesh 2, the velocity fluctuations in the shear layer (r/D=0,5 Figure 10b) develops slower but eventually reach the same values as the other

meshes at z/D=~1.

It is remarkable the difference between the three meshes in the near wall region. All meshes are identical for z/D<0,5 and have similar values for the turbulent variables for z/D>0,5 (see for example Figure 9 and Figure 10). Yet the results for the three meshes behave considerably differently approaching the wall. Only mesh 3 shows a rapid decrease in velocity fluctuations approaching the wall as is physically expected.

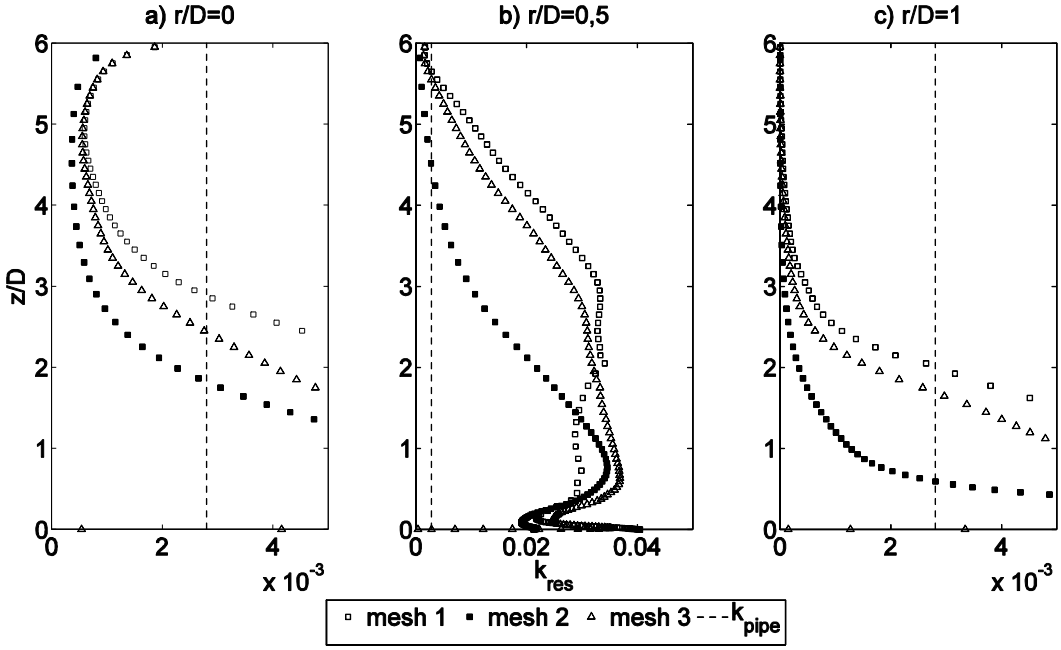

Figure 9: Effects of wall-normal cell distribution on resolved k (k_{res}). For reference fully developed pipe flow "k_{pipe}".

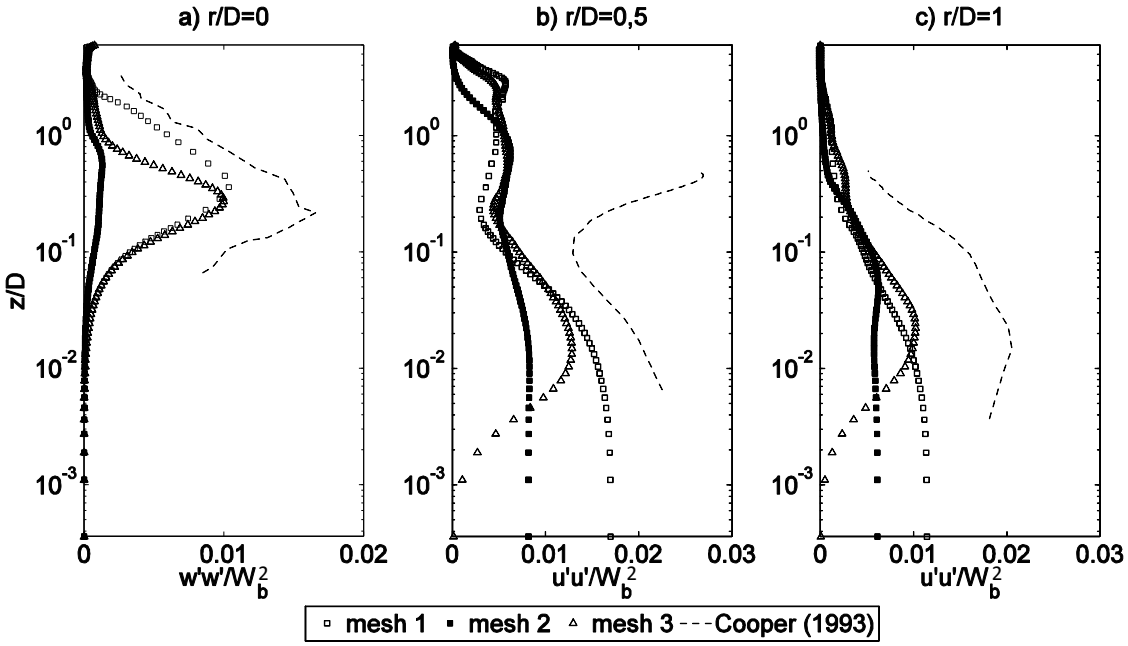

Figure 10: Effects of mesh wall-normal distribution on resolved velocity fluctuations. w' (wall normal) and u' (radial) velocity fluctuation.

The heat transfer prediction for the simulations run with LES are plotted in Figure 11. All meshes give results relatively close to the experiments with up to about 25% local deviation. It can be observed as the results are fairly parallel to each other. Interestingly, there is not a trend correlation between Nu and magnitude of fluctuation close to the wall (for example compare Figure 10c and Figure 11 for r/D=1).

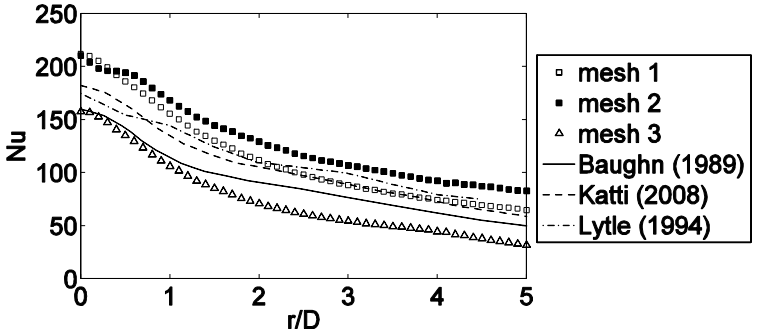

Figure 11: Effect of mesh wall-normal distribution on Nu.

Also the URANS models are tested with different wall-normal cell distribution. The remarkable result is that URANS models fail completely to predict the wall heat transfer using mesh 1 but work well with mesh 2 (Figure 13). A number of tests are conducted to identify the cause of this behavior. The same models are tested in their RANS implementation (steady state) and give results very close to the experiments with all meshes.

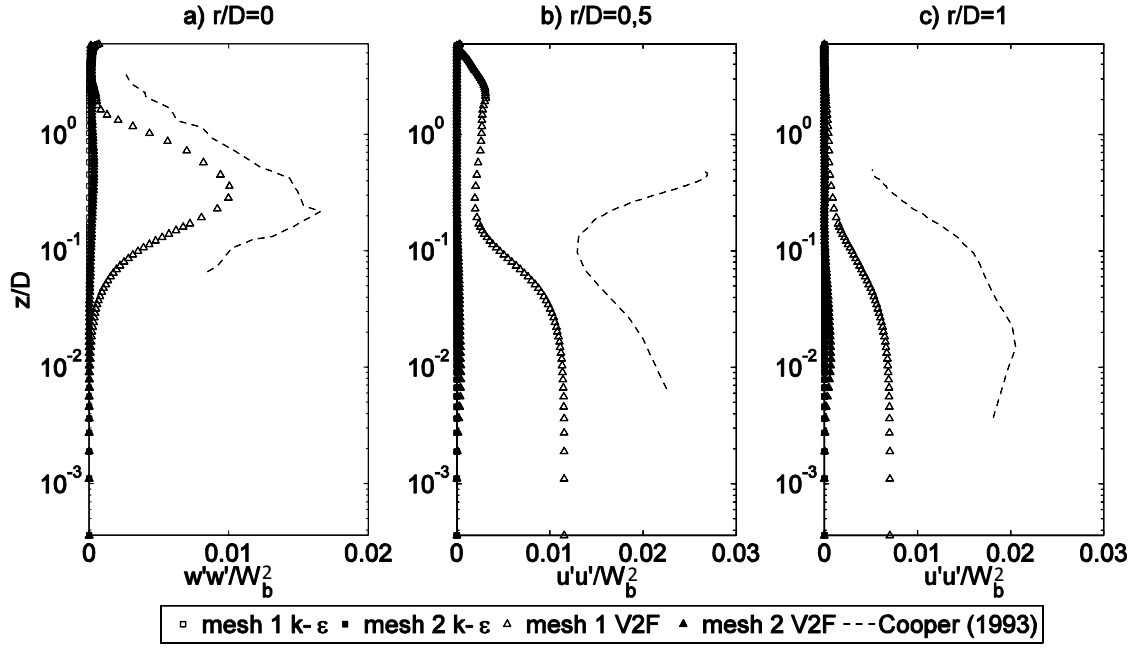

Figure 12 Effects of mesh wall-normal distribution on resolved velocity fluctuations for URANS models. w' (wall normal) and u' (radial) velocity fluctuation. Note: symbols overlap.

Further analysis reveals a correlation between the flow turbulent quantities and the predicted heat transfer. In Figure 12 it is possible to note that the turbulent fluctuations with the V2F model behave similarly to the LES model where, for mesh 1, turbulent quantities do not tend to zero approaching the wall. Notably, in the LES case the heat transfer prediction is satisfactory while the URANS models give unphysical results (Figure 13).

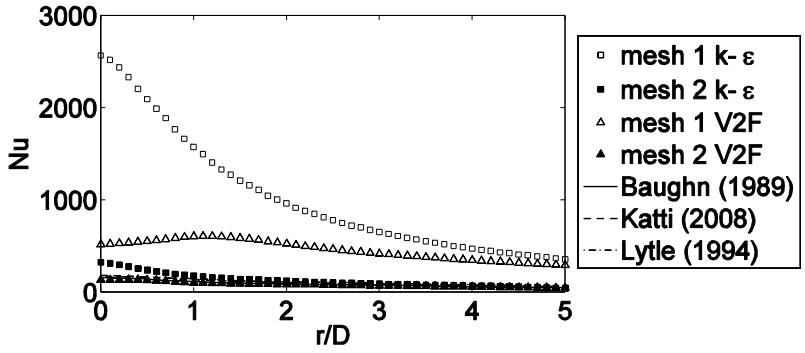

Figure 13 Mesh distribution effect on Nu using URANS models.

A possible explanation of the strong dependence of URANS models (k-ε and V2F) to the mesh wall-normal spacing could be as follows: if the mesh size is coarse, fluctuations are not resolved and the model behaves essentially in RANS mode. If instead the mesh is fine enough a larger part of the velocity fluctuations u' is resolved. Consequently higher velocity gradients are present in the flow and this increases the value of the strain tensor S_{ij}. This variable is active in the production term, P_k, of the k transport equation, which, in turns, increases the value of μ_t as shown in Figure 14.

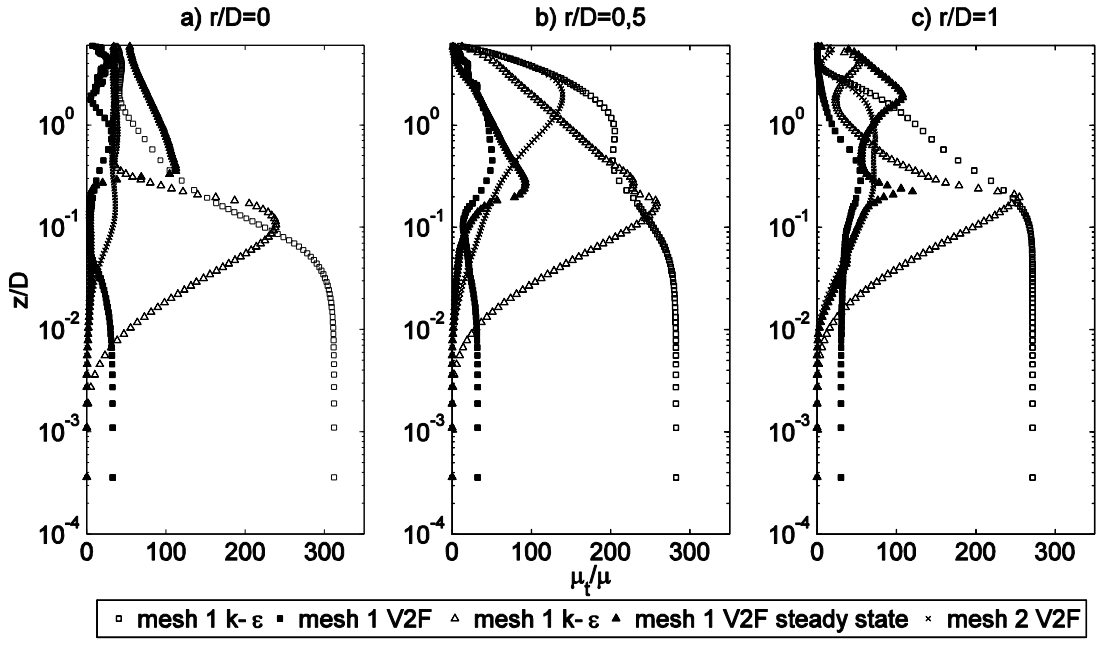

Figure 14: Turbulent viscosity μ_t development for RANS and URANS.

Although high, μ_t does not manage to damp sufficiently the velocity fluctuations approaching the wall and consequently the model fails to predict the heat transfer. The standard k-ε (not realizable) generates higher μ_t than the V2F model resulting in a larger over-prediction of the heat transfer (Figure 13), despite dampening the velocity fluctuation more effectively (Figure 12). The behavior is confirmed by comparing the development of μ_t for RANS and URANS (Figure 14). Indeed, in the RANS case no fluctuations are resolved by definition and μ_t goes to zero for both models (k-ε and V2F) bringing heat transfer prediction close to the experimental data.

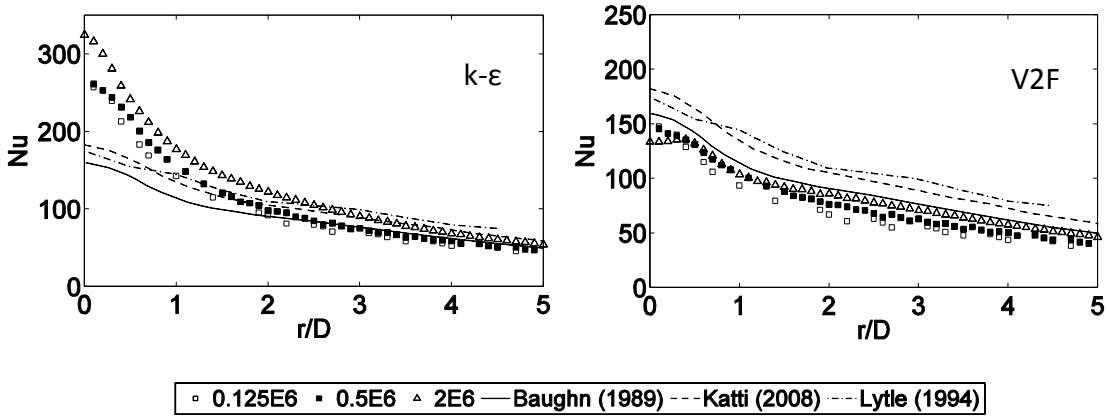

Figure 15: Effect of mesh density in wall-parallel direction on the Nu with URANS. Spacing based on mesh 2.

The effect of the mesh density in wall-parallel direction for the k-ε and V2F model can be seen in Figure 15. Three different meshes are tested with 0.125e6, 0.5e6 and 2e6 cells, these are obtained refining the coarsest mesh only in angular and radial direction. Mesh 2 is used as reference for wall-normal spacing.

The V2F model gives results close to the experimental data. It can be seen that the Nu slightly increases with increasing cell density driving results with the k-ε model farther away from experimental data.

3.3 Computational cost

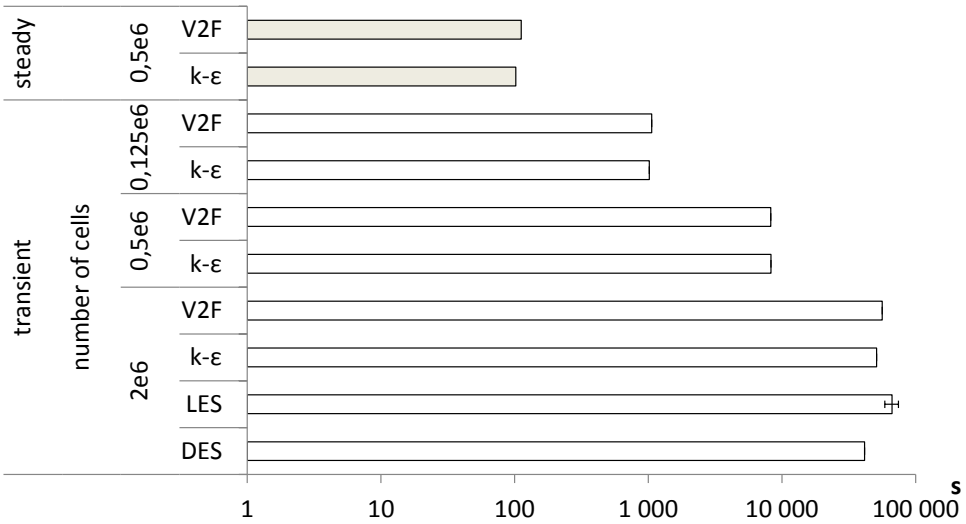

Figure 16: CPU real time per simulated second. More than one simulation is run with the LES model, the error bar is the standard deviation.

Figure 16 presents the time necessary for one CPU to compute one second of simulated time. This time is affected by many factors such as the number and type of CPUs used. Another important factor is the need to solve extra subroutines. These are for example the two extra subroutines used for the implementation and post processing of the synthetic fluctuation. In parallel computing, communication between CPUs is a significantly time-consuming process. The domain is partitioned in groups of cells and each group is assigned to a CPU. At

the end of each iteration, the solution at the cell group boundaries needs to be passed to the CPU(s) computing for the adjacent group.

For the reasons presented above, the data from Figure 16 can be treated only as indicative. It can be noticed that the V2F is slightly slower than the k-ε model. This is probably due to the fact that the V2F model solves for two extra equations. Nine simulations use the LES model with the same CPU configuration. The standard deviation for the runtime of these simulations is about 11%. In Figure 16 the computational cost related to the growing number of cells can also be appreciated. Computation time for steady state simulations is shown for comparison.

4 Conclusions

The URANS models are found to be very sensitive to the mesh wall-normal distribution. For most meshes tried, URANS models act much like their respective steady state simulation comparing with [6]. In these cases, the k-ε model is verified to be not sufficiently accurate in predicting heat transfer in the impingement zone. The V2F model is slightly more computationally expensive but gives significantly better results, even with a relatively coarse mesh. On the other hand, the V2F model is more likely to diverge. If the mesh is sufficiently fine, the URANS models can resolve a significant part of the turbulent fluctuations. In this case it is shown that the k-ε model is more effective in dampening the velocity fluctuations than the V2F model. However, in this case, both models fail to give an accurate prediction of the heat transfer.

The LES model is studied more extensively, changing a number of parameters. This model is capable of resolving the turbulent structures in the shear layer in a satisfactory manner. The results are good both in terms of heat transfer prediction and flow-field turbulent characteristics. Only relatively little differences are noted when changing the various parameters. Also the LES model is found to be sensitive to the wall-normal cell distribution. The most remarkable effects of this are seen on the resolved velocity fluctuations in the near wall region. Unfortunately, LES simulations are inherently expensive, since they require both a fine mesh and a transient simulation, exponentially increasing the computational cost.

The inlet turbulence is mentioned by different authors as an important parameter on the heat transfer effect of impinging jet. In this work this effect is not verified. For the jet configuration tested (H/D=6 Re=23000) the turbulence generated by the shear layer reaches the jet potential core before the impingement. The shear layer turbulence is an order of magnitude higher than the inlet turbulence thus overwhelming its effects.

The objective of this work is to evaluate different approaches to the simulations of impinging jet flows. The test and cross-evaluation of many different models is useful when deciding how to address the modeling this kind of flow.

5 References

1. Baughn, J. W. and Shimizu, S. [1989], Heat transfer measurements from a surface with uniform heat flux and an impinging jet, ASME J. Heat Transfer 111/1097.
2. Katti, V.and Prabhu, S.V. [2008], Experimental study and theoretical analysis of local heat transfer distribution between smooth flat surface and impinging air jet from a circular straight pipe nozzle, Int. J. Heat Mass Transfer article in press.
3. Lytle, D. and Webb, B.W. [1994], Air jet impingement heat transfer at low nozzle plate spacings, Int. J. Heat Mass Transfer 37 1687–1697.

4. Yue-Tzu Yang, Shiang-Yi Tsai [2007], Numerical study of transient conjugate heat transfer of a turbulent impinging jet. Heat and Mass Transfer 50 799–807.
5. M. Angioletti a, E. Nino a, G. Ruoccob, CFD turbulent modelling of jet impingement and its validation by particle image velocimetry and mass transfer measurements, International Journal of Thermal Sciences 44 (2005) 349–356
6. M. Bovo et al., On the numerical modelling of impinging jet heat transfer, Int. Symp. on Convective Heat and Mass Transfer in Sustainable Energy, 2009, Tunisia
7. Cooper, D., Jackson, D. C., Launder, B. E. & Liao, G. X. 1993 Impinging jet studies for turbulence model assessment-I. Flow-field experiments. Int. J. Heat Mass Transf. 36, 2675–2684.
8. Thomas Hällqvist 2006, Large Eddy Simulation of Impinging Jets with Heat Transfer KTH Mechanics, SE-100 44 Stockholm, Sweden, dissertation thesis.
9. L. Davidson [2007], Using isotropic synthetic fluctuations as inlet boundary conditions for unsteady simulations. Advances and applications in Fluid Mechanics, Vol. 1 Issue 1 1 – 35
10. H. M. Hofmann, R. Kaiser, M. Kind, H. martin, Calculations of steady and pulsating impinging jets—an assessment of 13 widely used turbulence models, Numerical heat transfer, part b, 51: 565–583, 2007.